International Journal of
Molecular Sciences

MDPI

Article

Structure, Function and Dynamics of mCoral, a pH-Responsive Engineered Variant of the mCherry Fluorescent Protein with Improved Hydrogen Peroxide Tolerance

Athena Zitti [1], Ozan Aksakal [1], Danoo Vitsupakorn [1], Pierre J. Rizkallah [2], Halina Mikolajek [3], James A. Platts [4], Georgina E. Menzies [1] and D. Dafydd Jones [1,*]

[1] Molecular Bioscience Division, School of Biosciences, Cardiff University, Sir Martin Evans Building, Cardiff CF10 3AX, UK
[2] School of Medicine, Cardiff University, Cardiff CF14 4XN, UK
[3] Diamond Light Source, Harwell Science & Innovation Campus, Didcot OX11 0DE, UK
[4] School of Chemistry, Cardiff University, Main Building, Cardiff CF10 3AT, UK
* Correspondence: jonesdd@cardiff.ac.uk; Tel.: +44-2920874290

Abstract

The red fluorescent protein mCherry is one of the most widely used fluorescent proteins in biology. Here, we have changed the chromophore chemistry by converting the thioether group of M66 to a thiol group through mutation to cysteine. The new variant, termed mCoral (due to its orange fluorescence hue), has similar brightness to mCherry but improved resistance to hydrogen peroxide. The variant is also responsive to pH with low and high pKa forms that have distinct spectral properties, which DFT analysis suggests is due to protonation state changes in the newly introduced thiol group, as well as the phenol group. The structure of mCoral reveals that the M66C mutation creates a space within the β-barrel structure that is filled by a water molecule, which makes new polar interactions, including the backbone carbonyl group of F65. Molecular dynamics simulations suggest that this additional water molecule, together with local solvation around the chromophore, could play a role in promoting planarity of the full conjugated system comprising the chromophore. The mCoral chromophore makes slightly more H-bonds with water than mCherry. The main water exit point for mCherry is also narrower in mCoral, providing a potential explanation for increased resistance to hydrogen peroxide. Overall, a small structural change to mCherry has resulted in a new fluorescent protein with potentially useful characteristics and an insight into the role of dynamics and water in defining the structure–function relationship in red fluorescent proteins.

Keywords: fluorescent proteins; protein engineering; protein dynamics; protein structure

Academic Editor: Ivo Crnolatac

Received: 26 November 2025
Revised: 19 December 2025
Accepted: 20 December 2025
Published: 23 December 2025

1. Introduction

Fluorescent proteins (FPs) have revolutionised molecular and cellular biology by allowing genetic tagging of defined targets, enabling non-invasive imaging of biological processes [1–3]. Among the many available FPs, mCherry [4] is one of the most widely used. This red FP, originally derived from the *Discosoma* sp. DsRed [5] FP, is a popular choice due to its relatively simple monomeric structure, brightness and photostability [4,6]. However, in common with many FPs, mCherry's fluorescence is influenced by environmental factors, including pH and reactive oxygen species (ROS), such as hydrogen peroxide.

The pH sensitivity of FPs is an important factor to consider, especially when imaging cellular compartments whose pH environments are different to the cytosol [7]. While the cytosol is normally around pH 7, the Golgi apparatus is lower, at pH 6.0–6.7, and endosomes and secretory vesicles are lower again, at pH 5.0–6.5, while lysosomes are around 4.5–5.0. The mitochondrial matrix samples a slightly higher pH regime (7.5–8.0). While being able to monitor processes in different compartments is important for understanding various cellular processes, such as secretion, autophagy, endocytosis, and cellular stress, the right FP needs to be selected for the job. While mCherry is thought to be relatively stable to mildly acidic conditions, with a reported pKa of 4.5 [4], it can be influenced by other factors such as fusion partner and local protein concentrations. Furthermore, the pH responsiveness of mCherry is not completely understood but is thought to solely involve protonation of the phenolic group of the chromophore (Figure 1a); at pH 7, the phenolate form dominates [4,8]. Given the importance of pH to biology [9,10], there has been a concerted effort to develop pH-responsive FPs that report on changes in cellular pH, of which most, such as SypHer [11,12], mKeima [13] and pHlorin [14–16], are fluorescent in the green–yellow range. These FPs have some drawbacks, such as a limited pH range (e.g., either high range or low range), have modest dynamic ranges and can be sensitive to reactive oxygen species, such as hydrogen peroxide.

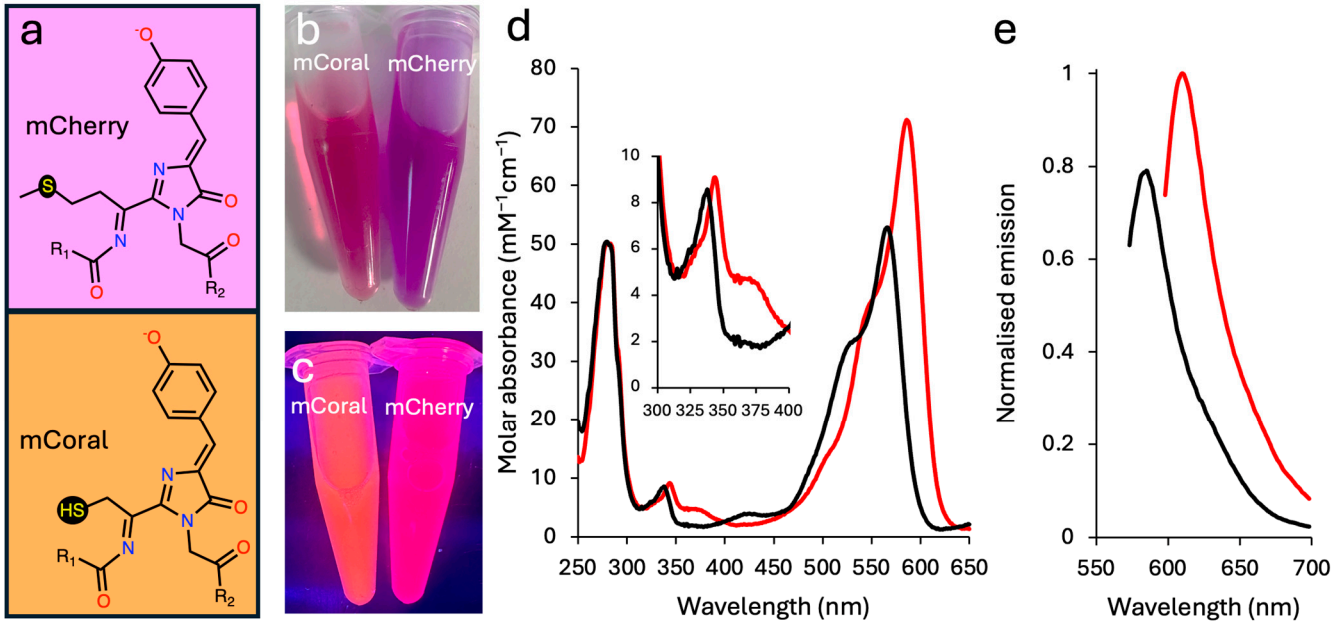

Figure 1. The effect of introducing cysteine into the mCherry chromophore. (**a**) The chromophore structures of mCherry (66-MYG-68 tripeptide) and the M66C variant (termed mCoral). The protein colours in: (**b**) ambient light and (**c**) on exposure to UV light. (**d**) The absorbance spectra of mCherry (red) and mCoral (black). The inset is the 300 to 400 nm region enlarged. (**e**) Emission spectra of mCherry (red) and mCoral (black) on excitation at their λ_{max} wavelengths in (**d**). Fluorescence emission (5 µM of each protein), normalised to mCherry based on their respective λ_{EM} values.

As well as pH flux, reactive oxygen species (ROS), like hydrogen peroxide, play an important role in biological systems [17,18] and can impact FPs' function [19]. Resistance to H_2O_2 is particularly important as it is generated as part of the chromophore maturation process [20–22], and the chromophores themselves can promote the further formation of H_2O_2 [23–25]. One of the design concepts for improved resistance to H_2O_2 is the removal of sulphur-containing amino acids, such as methionine and cysteine, as sulphur oxidation is a common mechanism of action [26]. H_2O_2 is also an important biological signalling molecule, leading to the construction of engineered FPs capable of detecting changes in

its level. These sensors, such as the HyPer series [27,28], are normally based on a domain insert system, with an H_2O_2-responsive protein, such as OxyR, inserted within an FP.

Here, we have taken the commonly used red fluorescent protein, mCherry [4,8] and converted it into a pH-responsive variant with improved resistance to H_2O_2. This new variant, termed mCoral, has a single mutation, M66C, within the chromophore-forming amino acid XYG sequence. Structure determination reveals that mCoral is similar to mCherry, but its chromophore has a different hydration pattern. Molecular dynamics (MDs) simulations suggest that the additional water molecule occupying the space left upon side chain shortening at residue 66 helps retain the extended chromophore planar state of the chromophore. MDs also reveal that water exit points differ between mCherry and mCoral, with the main exit point narrower in mCoral.

2. Results and Discussion

2.1. Generation of mCoral

The chromophore of typical β-barrel fluorescent proteins is comprised of the tripeptide sequence XYG, where the first amino acid is variable [3,29,30]. The CYG sequence is relatively uncommon as a chromophore-forming sequence, with less than 5% of FPs in FPBase [31] containing this tripeptide sequence; many of these derive from *Echinophyllia* Sp. 22G dronpa-based photoswitchable variants [32]. The majority of CYG chromophores also excite below 550 nm. Incorporation of cysteine within the chromophore does, however, open up the potential for new chemical properties not available to the other 19 common natural amino acids that can dynamically tune the spectral characteristics of an FP. These include redox activity [33,34], a physiologically relevant pKa (~8) [35], metal ion binding [36] and covalent modification [37]. We thus sought to introduce cysteine into the commonly used red FP, mCherry [4,8] via the M66C mutation, to form the chromophore outlined in Figure 1a.

Introduction of the M66C mutation results in a functional, fluorescent protein, but with a change in observable colour compared to parental mCherry (Figure 1b,c). In ambient light, mCherry turns from a dark purple to a burgundy hue on mutation of M66 to cysteine (Figure 1b). When irradiated with UV light, the M66C mutation results in mCherry turning from a pink to an orange coral colour (Figure 1c). For this reason, we now refer to the mCherry M66C variant as mCoral. Compared to mCherry, the absorbance and emission spectra are blue-shifted (Figure 1d,e and Table 1). The mCoral absorbance spectra have the characteristic double hump absorbance spectrum of mCherry (Figure 1d), but with λ_{max} shifted by 21 nm and the molar absorbance 0.73 fold of mCherry (Table 1 and Figure 1d). The brightness of mCoral is similar to mCherry due to an improved quantum yield (Table 1).

Table 1. Spectral properties of selective RFPs.

Variant	λ_{max} (nm)	Molar Absorbance ($mM^{-1}cm^{-1}$)	λ_{EX} (nm)	Quantum Yield	Brightness ($mM^{-1}cm^{-1}$)
mCherry [a,b]	587	72.0	610	0.22	15.84
mCoral (M66C) [b]	566	52.8	585	0.27	14.26
mTangerine [a]	568	38.0	585	0.30	11.4
mBanana [a]	540	6.0	553	0.7	4.2
mNectarine [a]	558	58.0	578	0.45	26.1

[a], available in FPBase [31]; [b], determined in this study.

Three other DsRed-derived FPs contain the following CYG chromophore: mTangerine [4], mBanana [4] and mNectarine [35]. The mCherry-derived mCoral compares

favourably to mTangerine and mBanana, with higher brightness primarily due to improved molar absorbance (Table 1). In contrast, the directly evolved mNectarine does appear to be a better protein in terms of brightness but is blue-shifted compared to mCoral [35]. Furthermore, the reported absorbance spectra at pH 7 for mNectarine is complex, with at least three major peaks observed, which is likely due to multiple ionisable chromophore forms being present. In comparison, mCoral has a more defined spectral profile at pH 7 (Figure 1d,e).

2.2. The Effect of pH on mCoral

We next looked at the effect of pH on the spectral properties of mCoral. Initially observed for original GFPs [38], the chromophore phenol group is known to sample both the phenolic (Ph-OH) and phenolate (Ph-O^-) over physiological pH ranges. For DsRed-derived FPs, the Ph-O^- state dominates at neutral pH despite the pKa of the tyrosine phenol group normally being 10.1, with the change in pKa due to the local protein environment stabilising the phenolate negative charge [8]. The spectral properties suggest three distinct species for mCoral. At neutral pH, the major absorbance (and excitation) peak lies at 566 nm (Figure 2a,b). At higher pH (>9), the major absorbance (and excitation) peak blue shifts to 543 nm, with the major emission peak also blue shifted to 562 nm (Figure 2a,b); the absorbance spectrum at pH 8 shows a transition between the two forms. At lower pH (<5), a blue-shifted absorbance peak dominates at 420 nm (Figure 2a) that does not appear to have any significant fluorescence associated with it (Figure S1). Using the absorbance ratios of the major peaks at each pH, we calculated two pKa values for mCoral to be 5.7 and 8.8 (Figure 2c,d). When repeated with mCherry, there is no shift in peak wavelengths and only a drop in the peak intensity (Figure S2). A single pH transition is observed for mCherry with a pKa of 4.4 (Figure S2), which is similar to that reported previously (pKa 4.5) [4].

To try and understand the basis by which pH affects mCoral, we performed density function theory (DFT) calculations on each of the ionised states of the chromophore using the experimentally determined chromophore structure (*vide infra* for mCoral). The chromophore is isolated from the crystal structure and capped as amides in the position of flanking residues. Each possible protonation state is constructed, fully geometry optimised, and an absorption spectrum predicted. When we compare the DFT predicted absorbance values for each of the charged forms of the mCoral chromophore, the low pH form is likely to be the protonated C_{66}-SH/Y67-Ph-OH form (predicted lmax 422 nm; Table 2). The high pH form is likely to be the deprotonated thiolate–phenolate (C66-S^-/Y67-Ph-O^-, predicted λ_{max} 541 nm; Table 2). At neutral pH, two forms are possible: the thiolate–phenolic (C66-S^-/Y67-Ph-OH) or the thiol–phenolate (C66-SH/Y67-Ph-O^-). Given that the pKa for the phenolic–phenolate transition is known to lie in the pH 4–6 range for many β-barrel FP proteins [38,39], such as mCherry [8], and coupled with the DFT prediction that the major absorbance for C66-SH/Ph-O^- is closer to the observed λ_{max} (557 nm versus 566 nm, respectively) than C66-S^-/Ph-OH (Table 2), we suggest that the neutral pH form is populated largely by the thiol–phenolate chromophore form. The overall suggested pH conversion scheme is shown in Figure 2e. For mCherry, the Ph-OH is predicted to be absorbed at 438 nm with relatively weak oscillator strength, which would appear to be the origin of the new low intensity peak observed in the absorbance spectrum at pH 4.5 (Figure S2).

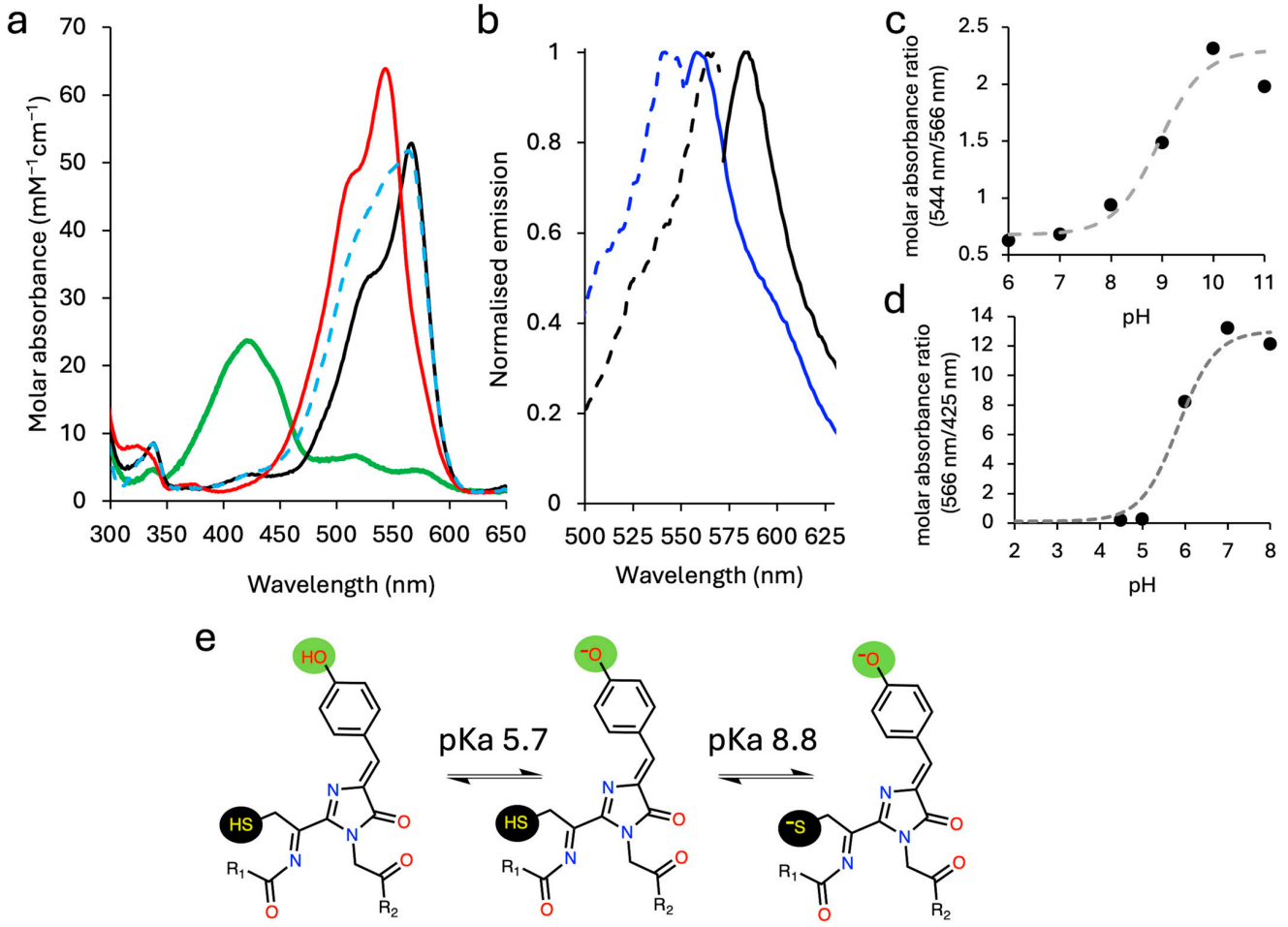

Figure 2. The pH-dependent spectral profile of mCoral. (**a**) The absorbance spectra of mCoral at pH 4.5 (green), pH 7 (black), pH 8 (dashed blue line) and pH 10 (red). (**b**) The excitation (dashed lines; emission at 580 nm) and emission spectra (solid lines; on excitation at the variant's λ_{max}) of mCoral at pH 10 (blue) and pH 7 (black). Emission is normalised to the pH 7 values. (**c**) The ratio plot of absorbance at 544 nm and 566 nm at pH 6 to 11 to determine the high-range pKa. (**d**) The ratio plot of absorbance at 566 nm and 425 nm at pH 4.5 to 8 to determine the low-range pKa. (**e**) The proposed model for different ionised states of mCoral chromophore, giving rise to the different spectral forms. The pKa values were calculated based on the plots in (**c**,**d**).

Table 2. Predicted maximal absorbance wavelengths for each chromophore ionised state.

Variant	Chromophore State	λ_{max}/S_0-S_1 (nm)	Oscillator Strength
mCherry	Ph-OH	438	0.21
	Ph-O^-	584	1.72
mCoral	C_{66}-SH/Ph-OH	422	1.26
	C_{66}-S^-/Ph-OH	601 440	0.06 1.32
	C_{66}-SH/Ph-O^-	557	1.69
	C_{66}-S^-/Ph-O^-	541	0.96

Insight into the origin of blue/red shifts resulting from pH changes can be drawn from the analysis of individual orbitals involved. All strong excitations are dominated by the highest occupied molecular orbital (HOMO) to the lowest unoccupied molecular orbital (LUMO) excitation, so this analysis focuses on these. In the fully protonated form, the

HOMO is localised mainly on the phenol and heterocycle, while the LUMO lies closer to the cysteine, with an energy difference between frontier orbitals ΔE = 3.2 eV. Deprotonating at phenol does not strongly change the localisation of orbitals and hence raises the energy of the HOMO more than that of the LUMO to give ΔE = 2.7 eV, consistent with the red shift seen at neutral pH. Further deprotonation at SH further raises the energy of both the HOMO and LUMO, but now affects the LUMO more due to its proximity to cysteine, resulting in ΔE = 2.84 eV, and so predicts a blue shift compared to SH/O- species.

2.3. Influence of H_2O_2 on mCoral Spectral Properties

Sulphur-containing amino acids, such as methionine and cysteine, can be chemically oxidised by biologically relevant reactive oxygen species (ROS), such as hydrogen peroxide [40,41]. Thus, the presence of a methionine (mCherry) or cysteine (mCoral) in the chromophore can have its disadvantages and advantages. The disadvantages include loss of fluorescence and thus cellular detection on chemical modification, but this can also be advantageous, as such modifications could result in changes to spectral properties, leading to the ability to sense these important ROS species [33,34,37].

Both mCherry and mCoral are sensitive to H_2O_2, but to different extents. With regards to their spectral properties, mCoral is more stable to H_2O_2 compared to mCherry (Figure 3a–c). After 1 h in 0.1% (*v*/*v*) H_2O_2, mCoral loses less than ~10% of its fluorescence emission, while mCherry's drops by ~35% (Figure 3a). The fluorescence emission of mCherry is effectively lost at 1 h in 0.5% (*v*/*v*) H_2O_2, while mCoral still retains ~35% of its signal after 1 h in 1% (*v*/*v*) H_2O_2 (Figure 3b). The absorbance spectra confirm there are significant changes to the chromophore on exposure to H_2O_2 (Figure 3c). The major absorbance peaks are lost for mCherry, suggesting loss of chromophore integrity, while mCoral still retains its absorbance peaks, albeit at a lower level (Figure 3c). In line with fluorescence, absorbance at λ_{max} suggests mCoral is more resilient to H_2O_2 than mCherry under similar conditions (Figure 3d).

To understand the chemical modification process likely to be driving the spectral changes, we determined the mass before and after H_2O_2 addition (Figures 3e and S3). For both proteins, when taking into account N-terminal methionine removal and chromophore maturation, the expected molecular mass is observed prior to the addition of H_2O_2. On addition of H_2O_2, both lose 58–59 Da in mass. We currently do not know what process is occurring for both proteins to lose a similar amount of mass, especially as the most common oxidation event involving sulphur-containing amino acids is oxygenation of the sulphur atom [40,41], which would increase the mass in units of 15–16 Da. Given that the loss in mass is the same for both proteins, we suggest that a common chemical event is occurring but is either occurring quicker in mCherry or has less of an impact in mCoral, based on the effect of H_2O_2 in spectral properties (Figure 3a–d). It has been reported that oxidation of cysteine is quicker than methionine [42,43], which seems at odds with our observations. One potential oxidative modification route reported recently is loss of the chromophore phenol group through cleavage at the β-methylene bridge [44], which could occur in combination with Cys/Met oxidation. We also cannot rule out secondary modification events outside of the chromophore occurring alone or in combination with Met/Cys oxidation. These could include conversion of arginine (e.g., R96) to glutamic–semialdehyde, proline (P63) ring opening [45] and/or glutamate (e.g., E215) decarboxylation [46] of residues close to the chromophore. Further mass spectrometry analysis or structure determination could provide an explanation for the H_2O_2-induced mass decrease.

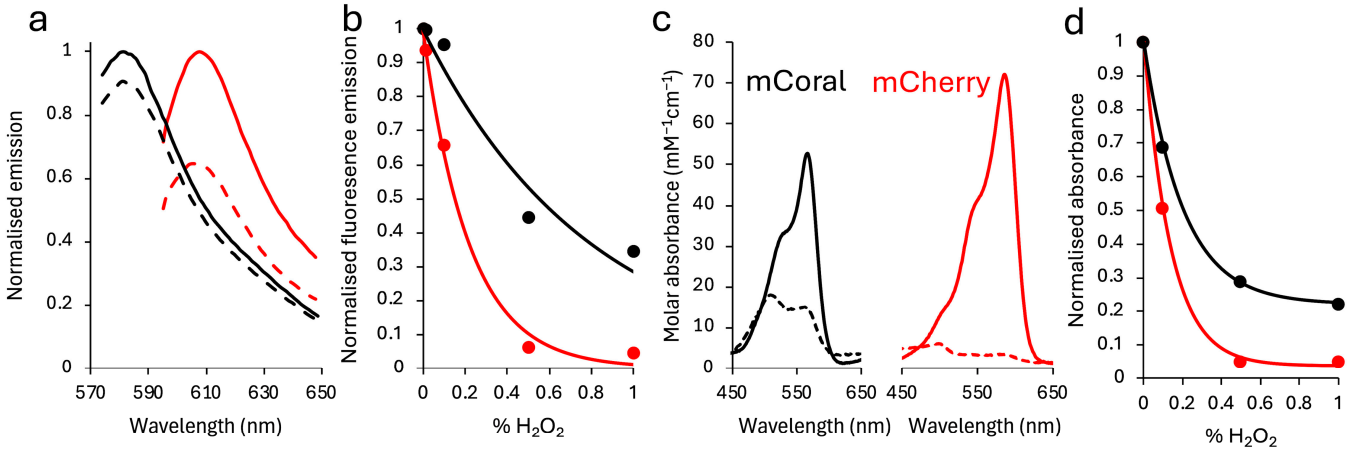

e

Protein	Expected mass (Da)	Measured mass (Da) No H_2O_2	Measured mass (Da) Plus H_2O_2	Difference (Da)
mCherry	27,669 27,537 (−N-Met)	27,537	27,479	−58
mCoral	27,641 27,509 (−N-Met)	27,509	27,450	−59

Figure 3. The effect of H_2O_2 on the spectral properties of mCoral (black) and mCherry (red). (**a**) The change in fluorescence emission before (solid lines) and after 1 h incubation of 5 μM protein with 0.1% (*v*/*v*) H_2O_2 (dashed lines). (**b**) Fluorescence emission on incubation of 5 μM protein for 1 h with different concentrations of H_2O_2. (**c**) Absorbance spectra before (solid lines) and after 1 h 0.5% (*v*/*v*) H_2O_2 (dashed lines). (**d**) The change in absorbance on incubation of 2.5 μM protein for 1 h with different concentrations of H_2O_2. The values were normalised to absorbance at 0% H_2O_2 at the protein's λ_{max}. (**e**) summary of expected versus observed protein masses before and after the addition of 0.1% (*v*/*v*) H_2O_2. Mass spectra can be found in Supplementary Figure S3.

2.4. Structure and Dynamics of mCoral

To understand how replacing methionine with cysteine in the mCherry chromophore affects spectral properties, we determined the structure of mCoral (see Table S1 for statistics). Overall, the M66C mutation does not change the general protein structure compared to mCherry (Figure 4a), with the Cα root mean square deviation (RMSD) over the whole protein of 0.152 Å. The chromophore and local protein environment surrounding the mutation site are also largely similar (Figure 4b). Water molecules (W1 to W4 in Figure 4c) retain similar positions to those observed in mCherry. The loss of -SCH_3 group on conversion of methionine to cysteine will result in space becoming available for an additional moiety; based on observed electron density, we have modelled water (WM66C in Figure 4d) to take the place of the original M66 side chain component. This additional water makes a new set of polar contacts with the backbone carbonyl of F65, the new thiol group in the chromophore and the sidechain carboxamide group of Q42. This new water molecule may also help stabilise the negative charge on the thiolate at high pH, as there are no basic residues close by. When we assess potential tunnels through to the new thiol group, access points calculated by CAVER [47] are found to be relatively distant from the chromophore, located towards either of the two cap ends of the β-barrel structure (Figure 4e). One tunnel (coloured red in Figure 4e) exits between stand S10 and the region bisecting strand 7, comprising residues 140 to 143, which is a bulge-type loop in the crystal structure.

We then turned to molecular dynamics (MDs) to provide further insight into mCoral's structure–function relationship. As has been applied previously [48], our MDs simulations use a chromophore that includes F65 to incorporate the additional double bond formed on maturation (see Figure S4). The overall average Ca RMSD over 3 × 1000 ns production MDs

runs for mCoral is relatively stable (Figure S5), with an average RMSD of 0.13 ns ± 0.01, slightly lower than mCherry (0.16 ns ± 0.01). The per-residue Ca root mean square fluctuation (RMSF) remains similar except for the chromophore (CRO) and its adjacent residues (Figure 5a). The mCherry CRO has a higher flux (0.11 nm ± 0.04) over the simulations compared to mCoral (0.051 nm ± 0.01).

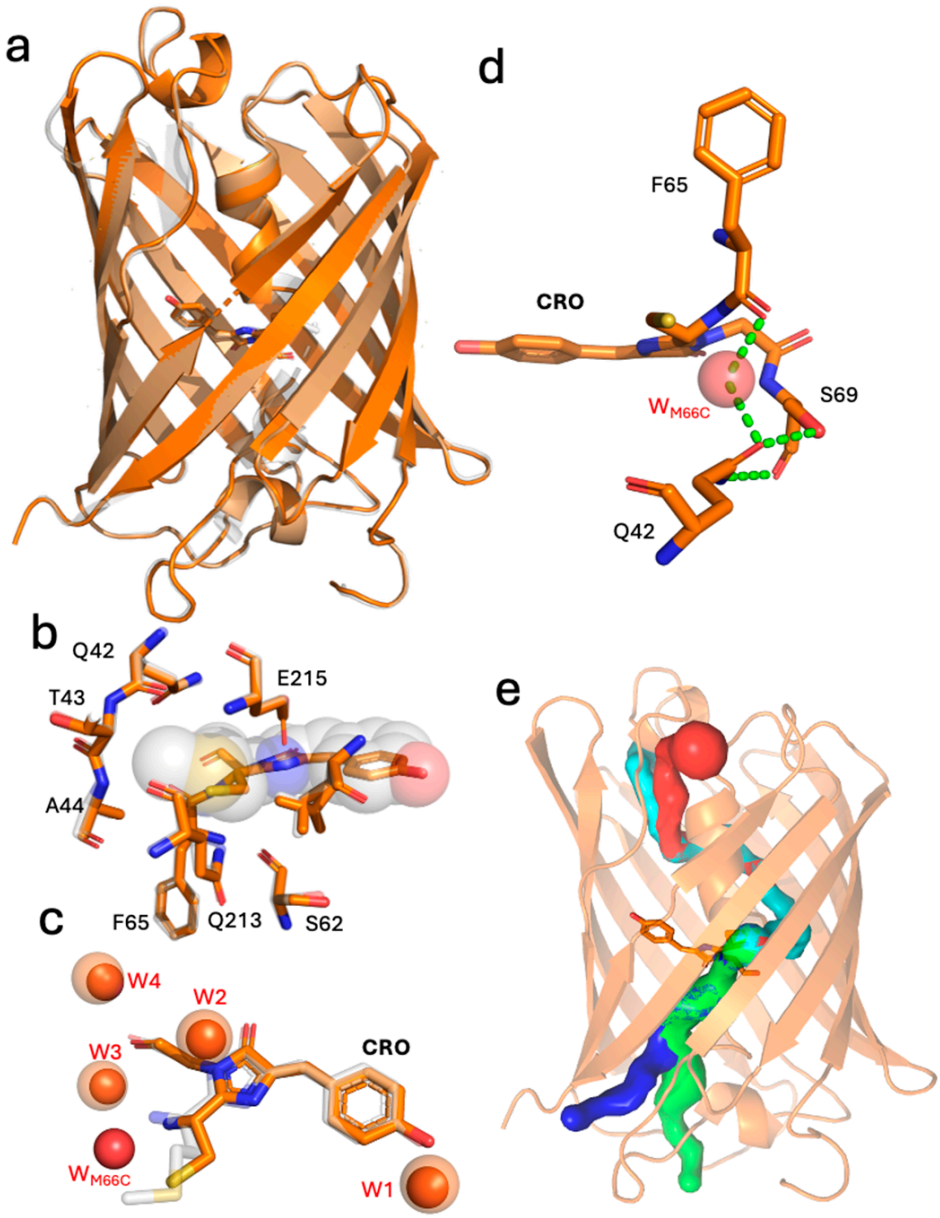

Figure 4. The structure of mCoral. (**a**) The structural alignment of mCoral (orange) and mCherry (grey; PDB 2h5q [8]). The chromophore is shown as sticks. (**b**) The structural alignment of mCoral local chromophore environment (orange) with that of mCherry (grey). The mCherry chromophore is shown as spheres and the mCoral chromophore as sticks. (**c**) Local water molecules surrounding chromophore in mCherry (chromophore shown as grey sticks, with waters represented as transparent orange spheres) and mCoral (chromophore shown as orange sticks, with waters represented as solid red spheres). (**d**) The polar network (shown as dashed green lines) involving water W_{M66C} (red sphere), calculated using the PyMOL 3 [49] polar contacts tool. (**e**) The calculated water tunnels into the void resulting from the M66C mutation. The tunnels (coloured blue, green, cyan and red) were calculated using CAVER3.0 [47].

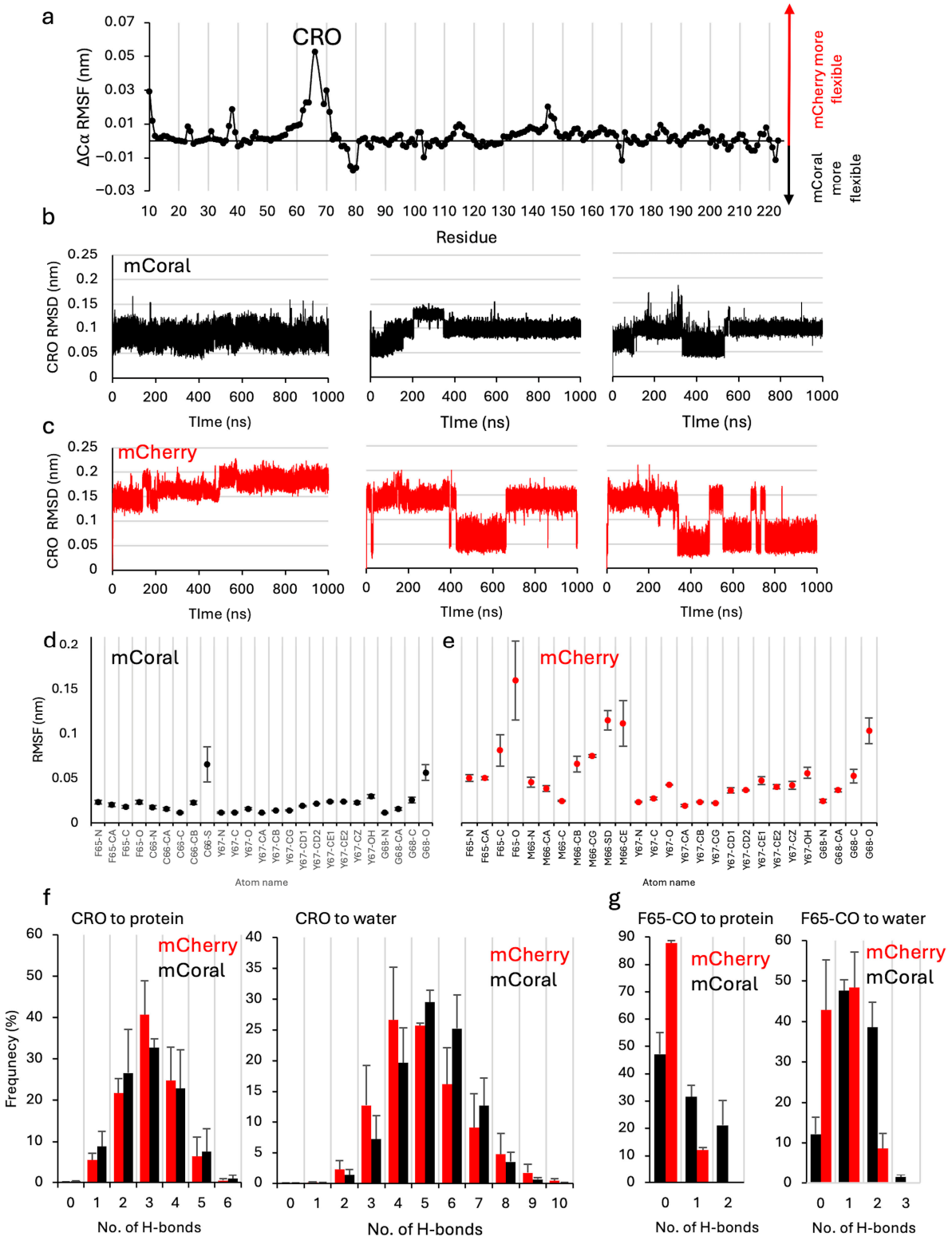

Figure 5. Molecular dynamics analysis of mCherry (red throughout) and mCoral (black throughout). (**a**) The difference in RMSF calculated by subtracting the mCoral residue Cα from the same residue of mCherry. The positive values represent a higher RMSF for mCherry, and negative values a higher RMSF for mCoral. The individual RMSF for each variant is shown in Figure S6. The CRO RMSD of the (**b**) mCoral and (**c**) mCherry. The per heavy atom CRO RMSF for (**d**) mCoral and (**e**) mCherry. The atom nomenclature is shown in Supplementary Figure S7. (**f**) The frequency of H-bonds between the CRO and either the rest of the protein or water. (**g**) The frequency of H-bonds between the carbonyl group of F65 and either the rest of the protein or water.

To probe CRO dynamics further, the RMSD of the chromophore (all atoms) was measured and found to differ between mCherry and mCoral (Figure 5b,c). RMSD analysis suggests that the mCherry CRO is switching between at least two distinct conformations. In comparison, mCoral's CRO appears more stable, with some alternative states observed but with RMSD fluxing to a lesser extent than that observed for mCherry. To identify the CRO atoms contributing to the step changes in RMSD, an atom-by-atom route mean square fluctuation (RMSF) was performed on the CRO (Figure 4d,e). For mCoral, the fluctuation of each atom was low (average of 0.022 nm ± 0.012), with the thiol sulphur of the newly introduced C66 (C66-S in Figure 5d) being the most dynamic atom. In contrast, mCherry displayed higher per-atom flux (0.054 nm ± 0.034). More specifically, the carbonyl oxygen from F65 (F65-O in Figure 5d,e) is highly dynamic in mCherry but is relatively stable in mCoral. As mentioned above, the F65 carbonyl oxygen forms interactions with the newly observed WM66C water molecule in mCoral (Figure 4d). This could suggest an important role for the WM66C water molecule in stabilising the chromophore conformation. As with mCoral, the side chain of the residue 66 component of the mCherry chromophore is also more dynamic than most of the chromophore heavy atoms (Figure 5e). This suggests that, despite being packed within the core of the protein, rotation of the -SCH3 group is possible in mCherry.

Given the potential importance of local polar interactions between the CRO and its protein and solvent environment (see Figure 4c,d), we measured the number and persistence of H-bonding involving the CRO in each variant. Throughout the simulations, the CRO makes extensive H-bonds with both the rest of the protein and water (Figure 5f), with an average of over 8×10^5 observed over each 1 μs (100,001 frames) MDs simulation for each protein. The mCherry CRO makes slightly more H-bonds with the rest of the protein (average of 3.1 × 105; 3.1 ± 0.3 per frame) compared to mCoral (average of 2.9×10^5; 2.9 ± 0.4 per frame). Both have a median value of three H-bonds to the rest of the protein, but the frequency of three or more H-bonds is higher for mCherry (Figure 5f). In contrast, mCoral makes slightly more H-bonds with water molecules (average of 5.3×10^5 versus 4.9×10^5; 5.3 ± 0.3 per frame versus 4.9 ± 0.6 per frame). The number of H-bonds with water spans a greater range, with the highest frequency interactions in mCoral at a higher H-bond count (5–6 H-bonds per frame) compared to mCherry (4–5 H-bonds per frame). When the carbonyl oxygen of F65 is assessed specifically, H-bonds are formed more frequently in mCoral with both protein and water (Figure 5g). On average, the mCoral carbonyl oxygen of F65 forms 6-fold and 2-fold more H-bonds with either the rest of the protein or water, respectively, than in mCherry. Thus, the introduction of the M66C mutation, coupled with the incorporation of a new water molecule, leads to changes in the local chromophore interaction network.

The isolation of representative individual trajectories of the different observed RMSD states shows that the F65 carbonyl oxygen flips position during the mCherry simulation (Figure 6a). In the high RMSD form, the carbonyl oxygen flips ~180° compared to the lower RMSD form, representative of the crystal structure conformation, resulting in the last double bond being out of plane with the rest of the conjugated network. Linked to the flip is the configuration of the M66 side chain, which changes the relative positions of the Cβ, Cχ and S atoms (Figure 6a). With respect to mCoral, there is rotation of the F65 carbonyl oxygen (up to 50°) but within the plane of the conjugated bond system (Figure 6b). The thiol sulphur also changes its positioning. DFT calculations performed on the alternate chromophore configuration identified for mCherry predict that the protonated form will absorb at 369 nm (strength 1.18), and the deprotonated form at 422 nm (strength 0.90), representing a significant blue shift compared to the dominant conformation. There is a low intensity and a weak absorbance peak at ~380 nm, only present in the mCherry spectrum

(Figure 1d, inset). However, given the frequency observed for the alternative mCherry CRO state in the MDs simulations, it may not be sampled as frequently or be as persistent in the protein in the solution, resulting in minimal changes to steady state spectral properties. The MDs simulations suggest that the M66C mutation stabilises the conformation of the chromophore, with the local water interactions likely to be playing a key role.

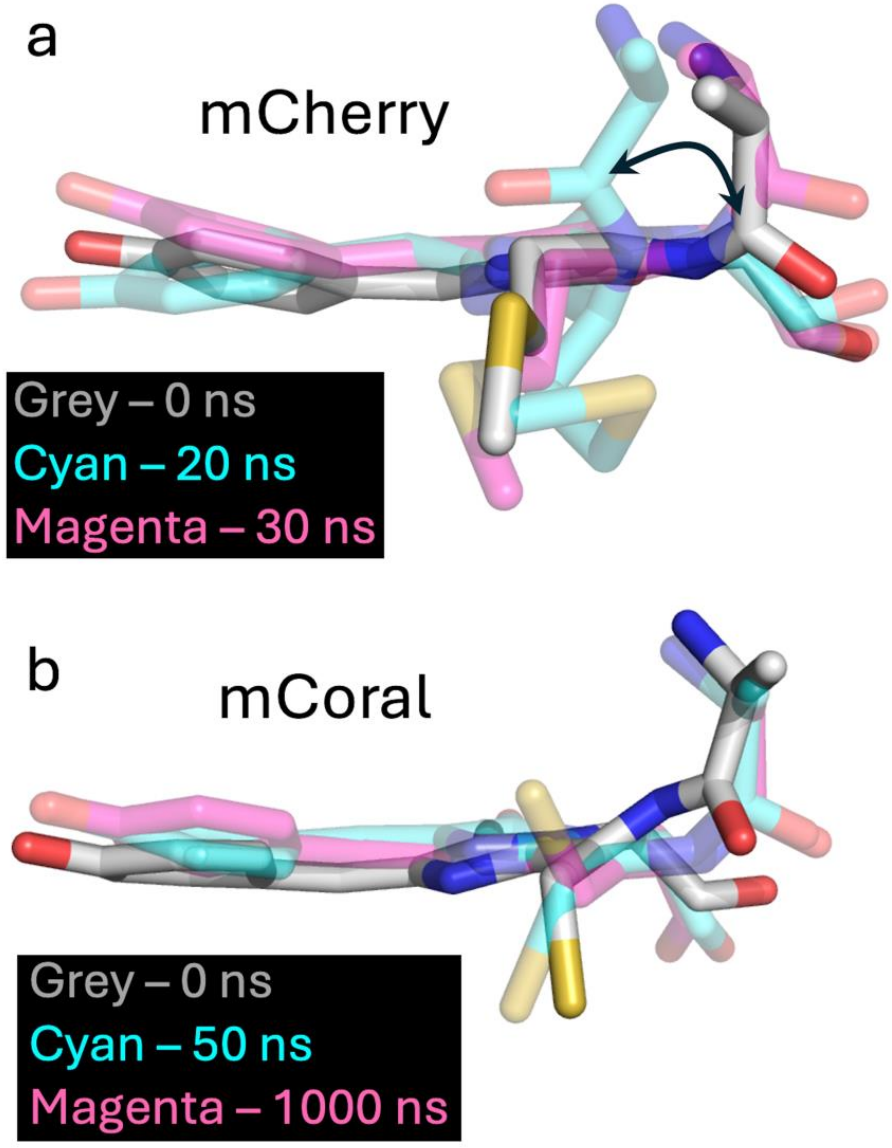

Figure 6. The different chromophore configurations of (**a**) mCherry and (**b**) mCoral extracted from 1000 ns simulations outlined in the figure. The structure for both was extracted from run two of the three 1000 ns MDs simulations. The colour of each conformation represents time points shown in the black boxes.

To mimic the experimentally observed solvated chromophore, we retained the original crystallographic waters during our simulations. To assess the impact of these water molecules, we reran the MDs simulations for mCherry, starting with the protein only (no crystallographic waters), allowing de novo solvation, including in and around the chromophore. Chromophore switching was observed in one 500 ns simulation, whereas switching was relatively rare in the other two 500 ns production runs (Figure S8). This suggests that the local water placement in mCherry could be influencing the exchange of the two F65 carbonyl oxygen states.

2.5. Chromophore-Associated Water Dynamics

We next looked at residency times and exit points of water molecules associated with the chromophore. The structurally conserved water molecule (W1 in Figure 4c) that H-bonds with the CRO phenol group in a wide range of FPs typically has a low residency [50], which also appears to be the case here (Table 3). The water resides longer in mCoral (average 6.2 ns ± 1.9) than mCherry (average 0.6 ns ± 0.3), but still rapidly exchanges with the bulk solvent. For mCherry, the local exit point for the W1 water is between the bulge interrupted strand S7 and strand S10. Indeed, this is the common exit point region for all the CRO associated waters in mCherry (Reg 1 and 2 in Table 3; Figure 7). In contrast, the water exit points vary for mCoral (Figure 7b). The CRO phenol-associated water can exit either side of the strand 7 bulge region, encompassing either strand S10 (Regs 1 or 2) or strand S8 (Reg 3). However, the most common water exit point is Reg 4, directly opposite the new thiol group, between strands S3 and S11 (Figure 7b and Table 3), which includes the new W_{M66C} water molecule. Indeed, while we hypothesised the importance of W_{M66C} in maintaining the chromophore structure, its residency time is relatively short (1.7 ns ± 1.7; Table 3).

Table 3. Water residency times and exit points.

Water	Run 1		Run 2		Run 3	
mCherry	Residency [a] (ns)	Exit [b]	Residency (ns)	Exit [a]	Residency (ns)	Exit [a]
W1	0.93	Reg 2	0.28	Reg 1	0.5	Reg 1
W2	93.33	Reg 2	122.05	Reg 1	164.2	Reg 2
W3	112.26	Reg 2	146.32	Reg 1	168.45	Reg 1
W4	114.84	Reg 1	128.37	Reg 1	495.34	Reg 1
W5	11.71	Reg 1	121.82	Reg 1	>10,000	N/A
W6	163.99	Reg 2	41.97	Reg 1	828.01	Reg 1
mCoral						
W_{M66C}	3.52	Reg 4	1.3	Reg 4	0.19	Reg 4
W1	7.1	Reg 1	4.07	Reg 1	7.6	Reg 3
W2	6.96	Reg 4	4.46	Reg 4	2.7	Reg 4
W3	2.52	Reg 4	130.24	Reg 2	9.06	Reg 4
W4	6.05	Reg 4	9.17	Reg 4	0.63	Reg 4
W5	6.04	Reg 4	8.01	Reg 4	4.58	Reg 4
W6	17.16	Reg 1	55.22	Reg 3	11.7	Reg 1

[a], Water residency times were determined by a distance that is consistently (≥0.1 ns) above a distance of 2 nm from the –β-methylene bridge atom. [b], Reg 1: between strands S7A-bulge (residues 139 and 145) and S10; Reg 2: between strands S7B (residue 146–153) and S10; Reg 3: between strands S7A-bulge and S8; Reg 4: between strands S3 and S11.

While chromophore-associated water residency does vary (with all but one exchanging with the bulk solvent), the lost waters are generally replaced by additional waters. This is highlighted by the persistence of H-bonds formed between the chromophore and water (Figure 5f). It still needs to be determined if water exchange rates are an important determinant of FP photophysical properties, but there is evidence that suggests it does [50–53].

To assess why the two proteins have different dominant water exit points, we looked at local interstrand distances. The exit point comprising strands S7 (regions S7A and S7B, linked by a short bulge) and S10 does appear to be consistently shorter in mCoral compared to mCherry (Figure 7c,d). This region is a known water exit point in other FPs, such as GFP [50,51]. The most frequently observed distance is ~0.8 nm for mCoral compared to ~1.1 nm for mCherry (Figure 7d). It has been suggested previously that lower distance fluctuation between strands S7 and S10 plays a role in improving photobleaching resistance

in the mCherry-XL variant (compared to mCherry) [53]. Given that mCoral also has shorter distance fluctuations in this region (Figure 4c,d), we speculate that this could contribute towards its improved resistance to H_2O_2.

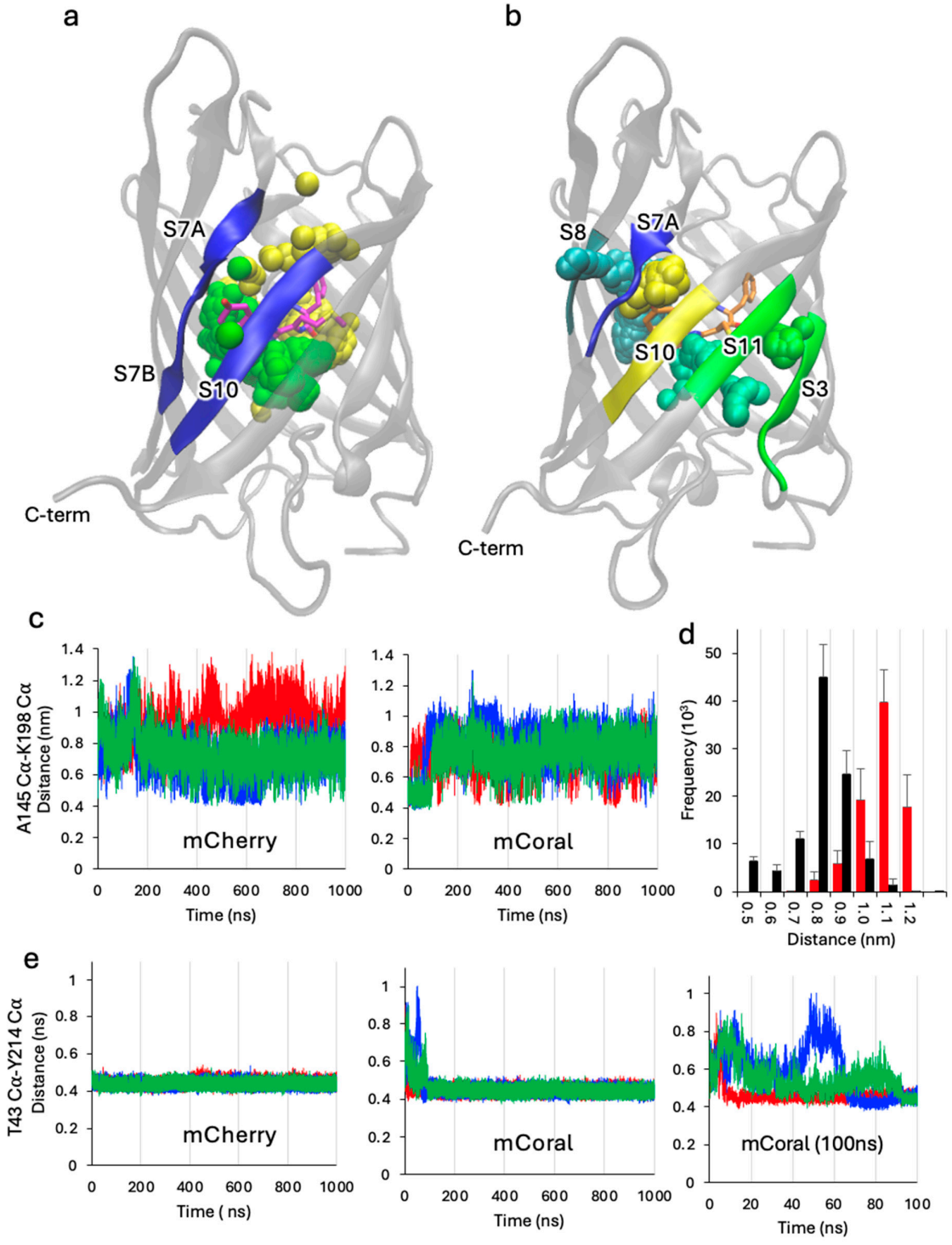

Figure 7. Chromophore-associated water dynamics. Representative water exit points for (**a**) mCherry and (**b**) mCoral. The different sphere colours represent different water molecular paths. (**c**) S7–S10 interstrand distances represented by the A145-K198 Cα distance. Green, blue and red represent the data from run 1, run 2 and run 3, respectively. (**d**) The distance distribution for mCherry (red) and mCoral (black) with bin sizes of 0.1 nm. (**e**) S3–S11 interstrand distances represented by the T43-Y214 Cα distance. Green, blue and red represent the data from run 1, run 2 and run 3, respectively. The rightmost panel is a zoom of the first 100 ns for the mCoral simulations.

Strand S10 is linked to S11, which, along with S3, forms a major water exit point for mCoral. In both proteins, the distance between strands S3 and S11 remains relatively stable (Figure 7e). However, the T43 (S3) and Y214 (S11) Cα distance in mCoral fluctuates within the first 100 ns before it stabilises. It is during this period of flux that water exchange occurs (Table 3), with no water exiting beyond 10 ns. Thus, local increased solvation on the introduction of the M66C mutation into mCherry does have repercussions in terms of local secondary structure stability. The new local solvent exit/entry point opposite the new thiol group may also contribute to mCoral's increased susceptibility to changes in pH.

3. Methods and Materials

3.1. Site-Directed Mutagenesis

The mCherry encoding gene resident in the pBAD bacterial expression plasmid has been described previously [54,55]. The M66C mutation was introduced by whole plasmid, inverse PCR using Q5 High Fidelity DNA polymerase kit (New England Biolabs, Ipswich, UK) in combination with forward (5′-GCTCCAAGGCCTACGTGAAG-3′) and mutagenic reverse (5′-CGTA**GCA**GAACTGAGGGGACA-3′; mutation site shown as bold and underlined) primers (synthesised by Integrated DNA Technologies), using the manufacturer's protocol. Plasmids were sequenced (EuroFins Genomics, Ebersberg, Germany) to confirm the presence of the mutation.

3.2. Recombinant Protein Production

The pBAD plasmids encoding mCherry or mCoral (mCherry M66C) were chemically transformed into *E. coli* TOP™ cells (Invitrogen Europe, Paisley, UK) and plated on LB agar plates supplemented with 50 μg/mL ampicillin. A single colony was used to inoculate a 5 mL overnight culture, which was then used to inoculate 2xTY media supplemented with 50 μg/mL ampicillin. The cultures were left to grow at 37 °C until they reached an OD_{600} of 0.6, when 0.2% (*v*/*v*) arabinose was added to induce expression. The cultures were left to incubate overnight at 37° in a shaking incubator. The cells were harvested via centrifugation at 5000× *g* for 20 min at 4 °C. The cell pellet was resuspended in 50 mM Tris-HCl buffer (pH 8), and the cells were lysed using a French press. The resulting lysate was clarified by centrifugation at 25,000× *g* for an hour at 4 °C, and the resulting supernatant was collected. Clarified cell lysate was loaded onto a 5 mL His-trap HP nickel affinity column (Cytiva, Amersham, UK), equilibrated in wash buffer (50 mM Tris-HCl, 10 mM imidazole pH 8.0) for Nickel-affinity chromatography. Bound protein was eluted by washing the column with 500 mM imidazole (pH 8.0). Pooled protein samples were then subjected to size exclusion chromatography (SEC), using a HiLoad 26/600 Superdex 200 column (Cytiva, Amersham, UK) that was equilibrated with 50 mM Tris-HCl buffer (pH8.0). The purity of the proteins was then checked by SDS-PAGE.

3.3. Spectral Analysis

Absorbance and fluorescence measurements were performed using a Cary 60 UV–Vis spectrophotometer (Agilent Technologies, Cheadle, UK) and a Varian Carry Eclipse Fluorescence spectrophotometer (Agilent Technologies), respectively. Absorbance spectra were recorded using a 1 cm path–length quartz cuvette. Protein fluorescence spectra were recorded using a 5 × 5 mm quartz cuvette, and data were collected with a 5 nm slit width at a rate of 600 nm/min. Each protein was excited at its respective excitation maximum. Spectra were recorded at concentrations of 2.5 μM or 5 μM. Molar absorbance for mCherry at its lmax was calculated to be similar to that reported in FPBase (https://www.fpbase.org/protein/mcherry/, accessed on 5 November 2025) and used to generate a molar absorbance (ε) value at 280 nm. The ε_{280} for mCherry was then used to

calibrate spectra for mCoral (as there are no additional aromatics present) to determine ε. The quantum yield of mCoral was determined as described previously [54], using mCherry as the standard. The pH profile analysis was performed as described previously [50] using 5 mM of protein at pH 4.5, 5.0, 5.5 (all 100 mM acetate buffer), 6.0 (100 mM KH_2PO_4), pH 7.0 (100 mM HEPES), 8.0 (50 mM Tris-HCl), 9.0, 10.0 (both 100 mM glycine-NaOH) and 11.0 (100 mM Na_2HPO_4-NaOH). Tolerance to H_2O_2 was determined using 2.5 (absorbance) or 5 mM (fluorescence) of protein mixed with increasing concentrations of H_2O_2 ranging from 0.01% (v/v) to 5% (v/v). Absorbance and fluorescence were recorded at various time intervals.

3.4. Mass Spectrometry Analysis

Pure mCherry and mCoral were diluted to 10 µM and analysed by the Mass Spectrometry facility in the School of Chemistry, Cardiff University. The sample was subject to liquid chromatography–mass spectrometry (LCMS) using a Waters Acquity UPLC/Synapt G2-Si QTOF mass spectrometer. For the H_2O_2-treated sample, H_2O_2 was added just prior to the LC step.

3.5. DFT Analysis

All DFT analysis employed the Orca 6.1.0 package [56]. Geometry optimisation used the PBE-D3BJ [57,58]/def2-SVP [59] level without any constraint, and confirmed as minima using harmonic frequency calculation. Absorption spectra and frontier molecular orbitals were then calculated at optimal geometry at PBE0 [60]/def2-TZVP level in the CPCM [61] model of aqueous solution. Orbital plots were obtained using Avogadro v 1.2.0.

3.6. mCoral Structure Determination

Crystal trials of purified protein samples (~10mg/mL) were set up at Diamond Light Source (DLS), Harwell, UK. Crystal formation was screened using sitting drop vapour diffusion across a wide variety of conditions, as described by the BSC, PACT, premierTM, JCSG-plusTM, SG1TM and MorpheusR crystallisation screens (Molecular Dimensions, Calibre Scientific, Rotherham, UK). Drops were set up with various protein–crystallisation buffer ratios, including 1:1, 1:2 and 2:1, using a mosquito (SPT) and left in Formulatrix imagers at VMXi to incubate at room temperature until crystals formed. Data were collected at VMXi and at I03. The process of crystallisation and data acquisition was automated at DLS. Crystals were formed under 0.2 M magnesium chloride, 0.1 M Tris buffer, pH 8, glycerol 10% v/v, 25% PEG 6–10kD and passed through the I03 DLS beamline. Following data acquisition, diffraction data were integrated and reduced using the XIA2 package [62]. The structure was solved by molecular replacement using PHASER, using the structure of mCherry (PDB 2H5Q as the search object using a process described previously) [63,64]. PHASER confirmed there was only one copy in the asymmetric unit, producing a large Log likelihood score of 6303 and TFZ (Twin Fraction Zero refinement) of 26, indicating high confidence in the result. The model was adjusted to match the correct sequences and to fit it into the electron density map using COOT [65] and then refined with TLS (Translation/Libration/Screw-rotation) parameters using RefMac5 [66,67]. All programs were accessed via the CCP4 package [68] (https://www.ccp4.ac.uk, accessed on 25 November 2025).

3.7. Molecular Dynamics Simulations

Molecular dynamics (MDs) simulations were performed on the Supercomputing Wales HAWK server (project code scw1631). Molecular dynamics were performed using GROMACS [69,70] and CHARMM27 forcefield [71,72], modified to contain constraints for the mCherry and mCoral chromophore in the CRO-O^- form. The forcefield parameters

are available on request. The protein was then placed centrally in a cubic box at least 1 nm from the box edge, applying periodic boundary conditions. The protein system was then solvated with water molecules (TIP3P) and the total charge balanced to zero with Na^+ ions. The protein was then energy minimised to below 1000 kJ mol^{-1} nm^{-1} with an energy step size of 0.01 over a maximum of 50,000 steps. The system was then temperature and pressure equilibrated using the NVT (constant number of particles, volume and temperature) followed by NPT (number of particles, pressure and temperature) ensembles. MDs production runs were then performed at 300 K, 1 atmosphere pressure for 1000 ns with a 2 fs time step integration. Each protein was subjected to 3 independent production runs. The original crystallographic waters present in the crystal structure were included in the 1000 ns production runs. The MDs process was repeated for mCherry with all crystallographic waters removed and added back de novo during the solvation step, with MDs production runs of 3 × 500 ns. The protein in the trajectories was centred in the simulation box, and dumps of individual trajectories were performed via the trjconv command. RMSD and RMSF calculations were performed using the rms and rmsf commands. Pairwise distances and hydrogen bonds were determined using the pairdist and hbond commands. The recommended H-bond default parameters were used (https://manual.gromacs.org/current/onlinehelp/gmx-hbond.html, accessed on 25 November 2025). Water residency times were determined by a distance that is consistently ($\geq$0.1 ns) above a distance of 2 nm from the β-methylene bridge atom.

4. Conclusions

Fluorescent proteins have proved to be pivotal in our understanding of biological processes, with mCherry being one of the most utilised FPs in the red region of the visible spectrum. The simple mutation of methionine to cysteine in the chromophore to generate mCoral adds new features to mCherry. Given the role of pH in biology [10,73], the pH-responsive nature of mCoral across a broad range opens up the possibility of it being used to monitor changes in different cellular compartments. mCoral could also be used in place of mCherry in environments where ROS levels are relatively high [74]. Indeed, it would be interesting to investigate in further studies if mutating M66 to serine, which is less susceptible to oxidation, would further improve tolerance to H_2O_2. While the M66C mutation has relatively little impact on protein structure, it does change two vital aspects: the water molecules local to the chromophore and the dynamics. Our long-time scale MDs of mCherry reveal that the chromophore itself could be undergoing conformational flux, switching between two distinct configurations. Such switching does not appear to be happening in mCoral, potentially due to a new water molecule that forms polar interactions with the carbonyl oxygen that undergoes the flip in mCherry. This has consequences in terms of future engineering of mCherry to improve its brightness. The quantum yield of FPs is thought to be influenced by the dynamics of the chromophore and surrounding residues [53,75], so engineering the next generation of brighter FPs in the red region could consider dynamics as part of the design process. The same is true for water dynamics. Internal waters molecules close to the chromophore help shape FPs' properties, with increased organisation likely playing a key role in improved brightness [50–52,54]. The next step is to understand how water dynamics are related to spectral properties. This, in turn, can help us establish rules to help predict how best to organise such waters through changes in the protein.

Supplementary Materials: The following supporting information can be downloaded at: https://www.mdpi.com/article/10.3390/ijms27010154/s1.

Author Contributions: A.Z. contributed to the conception of the project, generated the mCoral mutant, produced protein, undertook the spectral analysis, contributed to structure determination and contributed towards the molecular dynamics. O.A. contributed towards the molecular dynamics analysis and some aspects of mCherry characterisation. D.V. contributed to structure determination. P.J.R. contributed to structure determination. H.M. contributed to protein crystallisation and X-ray diffraction measurements. J.A.P. undertook DFT analysis. G.E.M. contributed towards molecular dynamics data generation and analysis and helped direct the project. D.D.J. contributed to project conception and directed the project, contributed to general data analysis and molecular dynamics analysis. All authors contributed to the writing of the paper and analysing data. All authors have read and agreed to the published version of the manuscript.

Funding: We would like to thank the EPSRC (EP/V048147/1) and BBSRC (International Partnership Award and BB/Z514913/1) for grant support. O.Z. was supported by an EPSRC DTP studentship. The Advanced Research Computing at Cardiff (ARCCA) facility (Hawk cluster) is part of Supercomputing Wales, part-funded by the European Regional Development Fund via the Welsh Government. This work was carried out with the support of Diamond Light Source instruments: VMXi (proposal mx29990) and I03 (proposal mx36446).

Institutional Review Board Statement: Not applicable.

Informed Consent Statement: Not applicable.

Data Availability Statement: The mCoral structure and associated data have been deposited in the Protein Data Bank under PDB ID 9TAD. All spectroscopic data will be made available via FigShare (to be released on publication).

Acknowledgments: The authors would like to thank the Cardiff School of Biosciences Protein Technology Hub for helping with the production and analysis of proteins. We would also like to thank the Advanced Research Computing at Cardiff (ARCCA) facility for supporting our molecular dynamics work. We would also like to thank Diamond Light Source, especially the VXMi facility and its staff, for the invaluable service they provide. We would like to thank the Crystallisation Facility at Harwell for access and support.

Conflicts of Interest: The authors declare no conflicts of interest.

References

1. Day, R.N.; Davidson, M.W. The Fluorescent Protein Palette: Tools for Cellular Imaging. *Chem. Soc. Rev.* **2009**, *38*, 2887–2921. [CrossRef]
2. Rodriguez, E.A.; Campbell, R.E.; Lin, J.Y.; Lin, M.Z.; Miyawaki, A.; Palmer, A.E.; Shu, X.; Zhang, J.; Tsien, R.Y. The Growing and Glowing Toolbox of Fluorescent and Photoactive Proteins. *Trends Biochem. Sci.* **2017**, *42*, 111–129. [CrossRef]
3. Shaner, N.C.; Steinbach, P.A.; Tsien, R.Y. A Guide to Choosing Fluorescent Proteins. *Nat. Methods* **2005**, *2*, 905–909. [CrossRef]
4. Shaner, N.C.; Campbell, R.E.; Steinbach, P.A.; Giepmans, B.N.G.; Palmer, A.E.; Tsien, R.Y. Improved Monomeric Red, Orange and Yellow Fluorescent Proteins Derived from Discosoma Sp. Red Fluorescent Protein. *Nat. Biotechnol.* **2004**, *22*, 1567–1572. [CrossRef]
5. Yarbrough, D.; Wachter, R.M.; Kallio, K.; Matz, M.V.; James Remington, S. Refined crystal structure of DsRed, a red fluorescent protein from coral, at 2.0-Å resolution. *Proc. Natl. Acad. Sci. USA* **2000**, *87*, 462–467. [CrossRef]
6. Cranfill, P.J.; Sell, B.R.; Baird, M.A.; Allen, J.R.; Lavagnino, Z.; De Gruiter, H.M.; Kremers, G.J.; Davidson, M.W.; Ustione, A.; Piston, D.W. Quantitative Assessment of Fluorescent Proteins. *Nat. Methods* **2016**, *13*, 557–562. [CrossRef]
7. Bizzarri, R.; Serresi, M.; Luin, S.; Beltram, F. Green Fluorescent Protein Based PH Indicators for in Vivo Use: A Review. *Anal. Bioanal. Chem.* **2009**, *393*, 1107–1122. [CrossRef] [PubMed]
8. Shu, X.; Shaner, N.C.; Yarbrough, C.A.; Tsien, R.Y.; Remington, S.J. Novel Chromophores and Buried Charges Control Color in MFruits. *Biochemistry* **2006**, *45*, 9639–9647. [CrossRef] [PubMed]
9. Madshus, I.H. Regulation of Intracellular PH in Eukaryotic Cells. *Biochem. J.* **1988**, *250*, 1–8. [CrossRef] [PubMed]
10. Casey, J.R.; Grinstein, S.; Orlowski, J. Sensors and Regulators of Intracellular PH. *Nat. Rev. Mol. Cell Biol.* **2010**, *11*, 50–61. [CrossRef]
11. Poburko, D.; Santo-Domingo, J.; Demaurex, N. Dynamic Regulation of the Mitochondrial Proton Gradient during Cytosolic Calcium Elevations. *J. Biol. Chem.* **2011**, *286*, 11672–11684. [CrossRef] [PubMed]

12. Matlashov, M.E.; Bogdanova, Y.A.; Ermakova, G.V.; Mishina, N.M.; Ermakova, Y.G.; Nikitin, E.S.; Balaban, P.M.; Okabe, S.; Lukyanov, S.; Enikolopov, G.; et al. Fluorescent Ratiometric PH Indicator SypHer2: Applications in Neuroscience and Regenerative Biology. *Biochim. Biophys. Acta (BBA) General. Subj.* **2015**, *1850*, 2318–2328. [CrossRef]
13. Kogure, T.; Karasawa, S.; Araki, T.; Saito, K.; Kinjo, M.; Miyawaki, A. A Fluorescent Variant of a Protein from the Stony Coral Montipora Facilitates Dual-Color Single-Laser Fluorescence Cross-Correlation Spectroscopy. *Nat. Biotechnol.* **2006**, *24*, 577–581. [CrossRef]
14. Mahon, M.J. PHluorin2: An Enhanced, Ratiometric, PH-Sensitive Green Florescent Protein. *Adv. Biosci. Biotechnol.* **2011**, *02*, 132–137. [CrossRef]
15. Miesenböck, G.; De Angelis, D.A.; Rothman, J.E. Visualizing Secretion and Synaptic Transmission with PH-Sensitive Green Fluorescent Proteins. *Nature* **1998**, *394*, 192–195. [CrossRef]
16. Sankaranarayanan, S.; De Angelis, D.; Rothman, J.E.; Ryan, T.A. The Use of PHluorins for Optical Measurements of Presynaptic Activity. *Biophys. J.* **2000**, *79*, 2199–2208. [CrossRef]
17. Sies, H. Role of Metabolic H2O2 Generation. *J. Biol. Chem.* **2014**, *289*, 8735–8741. [CrossRef] [PubMed]
18. Winterbourn, C.C. The Biological Chemistry of Hydrogen Peroxide. *Methods Enzymol.* **2013**, *528*, 3–25.
19. Shaner, N.C.; Lin, M.Z.; McKeown, M.R.; Steinbach, P.A.; Hazelwood, K.L.; Davidson, M.W.; Tsien, R.Y. Improving the Photostability of Bright Monomeric Orange and Red Fluorescent Proteins. *Nat. Methods* **2008**, *5*, 545–551. [CrossRef] [PubMed]
20. Auhim, H.S.; Grigorenko, B.L.; Harris, T.K.; Aksakal, O.E.; Polyakov, I.V.; Berry, C.; dos Gomes, G.P.; Alabugin, I.V.; Rizkallah, P.J.; Nemukhin, A.V.; et al. Stalling Chromophore Synthesis of the Fluorescent Protein Venus Reveals the Molecular Basis of the Final Oxidation Step. *Chem. Sci.* **2021**, *12*, 7735–7745. [CrossRef]
21. Craggs, T.D. Green Fluorescent Protein: Structure, Folding and Chromophore Maturation. *Chem. Soc. Rev.* **2009**, *38*, 2865–2875. [CrossRef]
22. Remington, S.J. Fluorescent Proteins: Maturation, Photochemistry and Photophysics. *Curr. Opin. Struct. Biol.* **2006**, *16*, 714–721. [CrossRef]
23. Ganini, D.; Leinisch, F.; Kumar, A.; Jiang, J.; Tokar, E.; Malone, C.C.; Petrovich, R.M.; Mason, R.P. Fluorescent Proteins Such as EGFP Catalytically Generate Superoxide Anion Free Radical and H2O2 in the Presence of NAD(P)H. *Free Radic. Biol. Med.* **2016**, *100*, S23. [CrossRef]
24. Bulina, M.E.; Chudakov, D.M.; Britanova, O.V.; Yanushevich, Y.G.; Staroverov, D.B.; Chepurnykh, T.V.; Merzlyak, E.M.; Shkrob, M.A.; Lukyanov, S.; Lukyanov, K.A. A Genetically Encoded Photosensitizer. *Nat. Biotechnol.* **2006**, *24*, 95–99. [CrossRef] [PubMed]
25. Trewin, A.J.; Berry, B.J.; Wei, A.Y.; Bahr, L.L.; Foster, T.H.; Wojtovich, A.P. Light-Induced Oxidant Production by Fluorescent Proteins. *Free Radic. Biol. Med.* **2018**, *128*, 157–164. [CrossRef]
26. Davies, M.J. Protein Oxidation and Peroxidation. *Biochem. J.* **2016**, *473*, 805–825. [CrossRef]
27. Belousov, V.V.; Fradkov, A.F.; Lukyanov, K.A.; Staroverov, D.B.; Shakhbazov, K.S.; Terskikh, A.V.; Lukyanov, S. Genetically Encoded Fluorescent Indicator for Intracellular Hydrogen Peroxide. *Nat. Methods* **2006**, *3*, 281–286. [CrossRef] [PubMed]
28. Pak, V.V.; Ezeriņa, D.; Lyublinskaya, O.G.; Pedre, B.; Tyurin-Kuzmin, P.A.; Mishina, N.M.; Thauvin, M.; Young, D.; Wahni, K.; Martínez Gache, S.A.; et al. Ultrasensitive Genetically Encoded Indicator for Hydrogen Peroxide Identifies Roles for the Oxidant in Cell Migration and Mitochondrial Function. *Cell Metab.* **2020**, *31*, 642–653.e6. [CrossRef]
29. Miyawaki, A.; Shcherbakova, D.M.; Verkhusha, V.V. Red Fluorescent Proteins: Chromophore Formation and Cellular Applications. *Curr. Opin. Struct. Biol.* **2012**, *22*, 679–688. [CrossRef]
30. Pakhomov, A.A.; Martynov, V.I. GFP Family: Structural Insights into Spectral Tuning. *Chem. Biol.* **2008**, *15*, 755–764. [CrossRef]
31. Lambert, T.J. FPbase: A Community-Editable Fluorescent Protein Database. *Nat. Methods* **2019**, *16*, 277–278. [CrossRef]
32. Ando, R.; Mizuno, H.; Miyawaki, A. Regulated Fast Nucleocytoplasmic Shuttling Observed by Reversible Protein Highlighting. *Science* **2004**, *306*, 1370–1373. [CrossRef]
33. Lohman, J.R.; Remington, S.J. Development of a Family of Redox-Sensitive Green Fluorescent Protein Indicators for Use in Relatively Oxidizing Subcellular Environments. *Biochemistry* **2008**, *47*, 8678–8688. [CrossRef]
34. Ostergaard, H.; Henriksen, A.; Hansen, F.G.; Winther, J.R. Shedding Light on Disulfide Bond Formation: Engineering a Redox Switch in Green Fluorescent Protein. *EMBO J.* **2001**, *20*, 5853–5862. [CrossRef] [PubMed]
35. Johnson, D.E.; Ai, H.; Wong, P.; Young, J.D.; Campbell, R.E.; Casey, J.R. Red Fluorescent Protein PH Biosensor to Detect Concentrative Nucleoside Transport. *J. Biol. Chem.* **2009**, *284*, 20499–20511. [CrossRef]
36. Jensen, G.C.; Janis, M.K.; Nguyen, H.N.; David, O.W.; Zastrow, M.L. Fluorescent Protein-Based Sensors for Detecting Essential Metal Ions across the Tree of Life. *ACS Sens.* **2024**, *9*, 1622–1643. [CrossRef] [PubMed]
37. Cloin, B.M.C.; De Zitter, E.; Salas, D.; Gielen, V.; Folkers, G.E.; Mikhaylova, M.; Bergeler, M.; Krajnik, B.; Harvey, J.; Hoogenraad, C.C.; et al. Efficient Switching of MCherry Fluorescence Using Chemical Caging. *Proc. Natl. Acad. Sci. USA* **2017**, *114*, 7013–7018. [CrossRef]
38. Tsien, R.Y. The Green Fluorescent Protein. *Annu. Rev. Biochem.* **1998**, *67*, 509–544. [CrossRef]
39. Remington, S.J. Green Fluorescent Protein: A Perspective. *Protein Sci.* **2011**, *20*, 1509–1519. [CrossRef] [PubMed]

40. Kim, G.; Weiss, S.J.; Levine, R.L. Methionine Oxidation and Reduction in Proteins. *Biochim. Biophys. Acta* **2014**, *1840*, 901–905. [CrossRef]
41. Garrido Ruiz, D.; Sandoval-Perez, A.; Rangarajan, A.V.; Gunderson, E.L.; Jacobson, M.P. Cysteine Oxidation in Proteins: Structure, Biophysics, and Simulation. *Biochemistry* **2022**, *61*, 2165–2176. [CrossRef]
42. Sjöberg, B.; Foley, S.; Cardey, B.; Fromm, M.; Enescu, M. Methionine Oxidation by Hydrogen Peroxide in Peptides and Proteins: A Theoretical and Raman Spectroscopy Study. *J. Photochem. Photobiol. B* **2018**, *188*, 95–99. [CrossRef]
43. Luo, D.; Smith, S.W.; Anderson, B.D. Kinetics and Mechanism of the Reaction of Cysteine and Hydrogen Peroxide in Aqueous Solution. *J. Pharm. Sci.* **2005**, *94*, 304–316. [CrossRef] [PubMed]
44. Bui, T.Y.H.; De Zitter, E.; Moeyaert, B.; Pecqueur, L.; Srinivasu, B.Y.; Economou, A.; Fontecave, M.; Van Meervelt, L.; Dedecker, P.; Pedre, B. Oxygen-Induced Chromophore Degradation in the Photoswitchable Red Fluorescent Protein RsCherry. *Int. J. Biol. Macromol.* **2023**, *239*, 124179. [CrossRef] [PubMed]
45. Amici, A.; Levine, R.L.; Tsai, L.; Stadtman, E.R. Conversion of Amino Acid Residues in Proteins and Amino Acid Homopolymers to Carbonyl Derivatives by Metal-Catalyzed Oxidation Reactions. *J. Biol. Chem.* **1989**, *264*, 3341–3346. [CrossRef]
46. Subach, F.V.; Verkhusha, V.V. Chromophore Transformations in Red Fluorescent Proteins. *Chem. Rev.* **2012**, *112*, 4308–4327. [CrossRef] [PubMed]
47. Chovancova, E.; Pavelka, A.; Benes, P.; Strnad, O.; Brezovsky, J.; Kozlikova, B.; Gora, A.; Sustr, V.; Klvana, M.; Medek, P.; et al. CAVER 3.0: A Tool for the Analysis of Transport Pathways in Dynamic Protein Structures. *PLoS Comput. Biol.* **2012**, *8*, e1002708. [CrossRef]
48. Laurent, A.D.; Mironov, V.A.; Chapagain, P.P.; Nemukhin, A.V.; Krylov, A.I. Exploring Structural and Optical Properties of Fluorescent Proteins by Squeezing: Modeling High-Pressure Effects on the Mstrawberry and Mcherry Red Fluorescent Proteins. *J. Phys. Chem. B* **2012**, *116*, 12426–12440. [CrossRef]
49. Schrödinger, L. The PyMOL Molecular Graphics System. 2020. Available online: https://www.pymol.org/support.html (accessed on 25 November 2025).
50. Ahmed, R.D.; Jamieson, W.D.; Vitsupakorn, D.; Zitti, A.; Pawson, K.A.; Castell, O.K.; Watson, P.D.; Jones, D.D. Molecular Dynamics Guided Identification of a Brighter Variant of Superfolder Green Fluorescent Protein with Increased Photobleaching Resistance. *Commun. Chem.* **2025**, *8*, 174. [CrossRef]
51. Shinobu, A.; Agmon, N. The Hole in the Barrel: Water Exchange at the GFP Chromophore. *J. Phys. Chem. B* **2015**, *119*, 3464–3478. [CrossRef]
52. Perticaroli, S.; Ehlers, G.; Stanley, C.B.; Mamontov, E.; O'Neill, H.; Zhang, Q.; Cheng, X.; Myles, D.A.A.; Katsaras, J.; Nickels, J.D. Description of Hydration Water in Protein (Green Fluorescent Protein) Solution. *J. Am. Chem. Soc.* **2017**, *139*, 1098–1105. [CrossRef] [PubMed]
53. Mukherjee, S.; Manna, P.; Douglas, N.; Chapagain, P.P.; Jimenez, R. Conformational Dynamics of MCherry Variants: A Link between Side-Chain Motions and Fluorescence Brightness. *J. Phys. Chem. B* **2023**, *127*, 52–61. [CrossRef]
54. Pope, J.R.; Johnson, R.L.; Jamieson, W.D.; Worthy, H.L.; Kailasam, S.; Ahmed, R.D.; Taban, I.; Auhim, H.S.; Watkins, D.W.; Rizkallah, P.J.; et al. Association of Fluorescent Protein Pairs and Its Significant Impact on Fluorescence and Energy Transfer. *Adv. Sci.* **2021**, *8*, 2003167. [CrossRef] [PubMed]
55. Reddington, S.C.; Driezis, S.; Hartley, A.M.; Watson, P.D.; Rizkallah, P.J.; Jones, D.D. Genetically Encoded Phenyl Azide Photochemistry Drives Positive and Negative Functional Modulation of a Red Fluorescent Protein. *RSC Adv.* **2015**, *5*, 77734–77738. [CrossRef]
56. Neese, F.; Wennmohs, F.; Becker, U.; Riplinger, C. The ORCA Quantum Chemistry Program Package. *J. Chem. Phys.* **2020**, *152*, 224108. [CrossRef] [PubMed]
57. Grimme, S.; Ehrlich, S.; Goerigk, L. Effect of the Damping Function in Dispersion Corrected Density Functional Theory. *J. Comput. Chem.* **2011**, *32*, 1456–1465. [CrossRef]
58. Perdew, J.P.; Burke, K.; Ernzerhof, M. Generalized Gradient Approximation Made Simple. *Phys. Rev. Lett.* **1996**, *77*, 3865–3868. [CrossRef]
59. Weigend, F.; Ahlrichs, R. Balanced Basis Sets of Split Valence, Triple Zeta Valence and Quadruple Zeta Valence Quality for H to Rn: Design and Assessment of Accuracy. *Phys. Chem. Chem. Phys.* **2005**, *7*, 3297. [CrossRef]
60. Adamo, C.; Barone, V. Toward Reliable Density Functional Methods without Adjustable Parameters: The PBE0 Model. *J. Chem. Phys.* **1999**, *110*, 6158–6170. [CrossRef]
61. Barone, V.; Cossi, M. Quantum Calculation of Molecular Energies and Energy Gradients in Solution by a Conductor Solvent Model. *J. Phys. Chem. A* **1998**, *102*, 1995–2001. [CrossRef]
62. Gildea, R.J.; Beilsten-Edmands, J.; Axford, D.; Horrell, S.; Aller, P.; Sandy, J.; Sanchez-Weatherby, J.; Owen, C.D.; Lukacik, P.; Strain-Damerell, C.; et al. Xia2.Multiplex: A Multi-Crystal Data-Analysis Pipeline. *Acta Crystallogr. D Struct. Biol.* **2022**, *78*, 752–769. [CrossRef]

63. Hartley, A.M.; Worthy, H.L.; Reddington, S.C.; Rizkallah, P.J.; Jones, D.D. Molecular Basis for Functional Switching of GFP by Two Disparate Non-Native Post-Translational Modifications of a Phenyl Azide Reaction Handle. *Chem. Sci.* **2016**, *7*, 6484–6491. [CrossRef]
64. Ahmed, R.D.; Auhim, H.S.; Worthy, H.L.; Jones, D.D. Fluorescent Proteins: Crystallization, Structural Determination, and Nonnatural Amino Acid Incorporation. In *Methods in Molecular Biology*; Humana Press Inc.: Totowa, NJ, USA, 2023; Volume 2564, pp. 99–119.
65. Emsley, P.; Cowtan, K. Coot: Model-Building Tools for Molecular Graphics. *Acta Crystallogr. D Biol. Crystallogr.* **2004**, *60*, 2126–2132. [CrossRef]
66. Winn, M.D.; Murshudov, G.N.; Papiz, M.Z. Macromolecular TLS Refinement in REFMAC at Moderate Resolutions. *Methods Enzymol.* **2003**, *374*, 300–321. [CrossRef]
67. Murshudov, G.N.; Vagin, A.A.; Dodson, E.J. Refinement of Macromolecular Structures by the Maximum-Likelihood Method. *Acta Crystallogr. D Biol. Crystallogr.* **1997**, *53*, 240–255. [CrossRef] [PubMed]
68. Collaborative Computational Project, N. 4. The CCP4 Suite: Programs for Protein Crystallography. *Acta Crystallogr. D Biol. Crystallogr.* **1994**, *50*, 760–763. [CrossRef] [PubMed]
69. Abraham, M.J.; Murtola, T.; Schulz, R.; Páll, S.; Smith, J.C.; Hess, B.; Lindahl, E. GROMACS: High Performance Molecular Simulations through Multi-Level Parallelism from Laptops to Supercomputers. *SoftwareX* **2015**, *1–2*, 19–25. [CrossRef]
70. Bekker, H.; Berendsen, H.J.C.; Dijkstra, E.J.; Achterop, S.; Van Drunen, R.; Van Der Spoel, D.; Sibjers, A.; Keegstra, H.; Renardus, M.K.R. GROMACS—A Parallel Computer For Molecular-Dynamics Simulations. *Phys. Comput.* **1993**, *7*, 252–256.
71. Brooks, B.R.; Brooks, C.L.; Mackerell, A.D.; Nilsson, L.; Petrella, R.J.; Roux, B.; Won, Y.; Archontis, G.; Bartels, C.; Boresch, S.; et al. CHARMM: The Biomolecular Simulation Program. *J. Comput. Chem.* **2009**, *30*, 1545. [CrossRef]
72. Best, R.B.; Zhu, X.; Shim, J.; Lopes, P.E.M.; Mittal, J.; Feig, M.; MacKerell, A.D. Optimization of the Additive CHARMM All-Atom Protein Force Field Targeting Improved Sampling of the Backbone φ, ψ and Side-Chain X1 and X2 Dihedral Angles. *J. Chem. Theory Comput.* **2012**, *8*, 3257–3273. [CrossRef]
73. Freeman, S.A.; Grinstein, S.; Orlowski, J. Determinants, Maintenance, and Function of Organellar PH. *Physiol. Rev.* **2023**, *103*, 515–606. [CrossRef] [PubMed]
74. Sies, H.; Belousov, V.V.; Chandel, N.S.; Davies, M.J.; Jones, D.P.; Mann, G.E.; Murphy, M.P.; Yamamoto, M.; Winterbourn, C. Defining Roles of Specific Reactive Oxygen Species (ROS) in Cell Biology and Physiology. *Nat. Rev. Mol. Cell Biol.* **2022**, *23*, 499–515. [CrossRef] [PubMed]
75. Goedhart, J.; Von Stetten, D.; Noirclerc-Savoye, M.; Lelimousin, M.; Joosen, L.; Hink, M.A.; Van Weeren, L.; Gadella, T.W.J.; Royant, A. Structure-Guided Evolution of Cyan Fluorescent Proteins towards a Quantum Yield of 93%. *Nat. Commun.* **2012**, *3*, 751. [CrossRef] [PubMed]